Journal of Solid State Chemistry 181 (2008) 3016–3023

Contents lists available at ScienceDirect

Journal of Solid State Chemistry

journal homepage: www.elsevier.com/locate/jssc

High-pressure modifications of $CaZn_2$, $SrZn_2$, $SrAl_2$, and $BaAl_2$: Implications for Laves phase structural trends

Subhadeep Kal [a,b], Emil Stoyanov [a], Jean-Philippe Belieres [a], Thomas L. Groy [a], Rolf Norrestam [c], Ulrich Häussermann [a,*]

[a] Department of Chemistry and Biochemistry, Arizona State University, P.O. Box 871604 Tempe, AZ 85287-1604, USA
[b] Department of Chemistry, Indian Institute of Technology, Kharagpur 721302, India
[c] Structural Chemistry, Stockholm University, 10691 Stockholm, Sweden

ARTICLE INFO

Article history:
Received 18 May 2008
Received in revised form
19 July 2008
Accepted 26 July 2008
Available online 8 August 2008

Keywords:
Polar intermetallic phases
$CeCu_2$ structure type
High pressure
Laves phases
Electron concentration controlled structural stability

ABSTRACT

High-pressure forms of intermetallic compounds with the composition $CaZn_2$, $SrZn_2$, $SrAl_2$, and $BaAl_2$ were synthesized from $CeCu_2$-type precursors ($CaZn_2$, $SrZn_2$, $SrAl_2$) and $Ba_{21}Al_{40}$ by multi-anvil techniques and investigated by X-ray powder diffraction ($SrAl_2$ and $BaAl_2$), X-ray single-crystal diffraction ($CaZn_2$), and electron microscopy ($SrZn_2$). Their structures correspond to that of Laves phases. Whereas the dialuminides crystallize in the cubic $MgCu_2$ (C15) structure, the dizincides adopt the hexagonal $MgZn_2$ (C14) structure. This trend is in agreement with the structural relationship displayed by *sp* bonded Laves phase systems at ambient conditions.

1. Introduction

Polar intermetallics are *sp* bonded compounds formed between an active metal component (which is an alkali, alkaline earth, or rare earth metal) and a more electronegative *p*-block or group 12 metal component [1,2]. Structurally and electronically they bridge charge balanced, often semiconducting Zintl phases and fully delocalized metallic systems. Although polar intermetallics still feature a polyanionic substructure, the clear relationship between electron count and atom arrangement of the polyanionic substructure typical of Zintl phases is gradually lost. Frequently, polar intermetallics realize the same structure type for a flexible range of electron counts, indicating that the significance of the electronic contribution to total energy is weakened [3]. The transition from polyanionic structures to close-packed arrangements is especially seen in systems AB_2 (A = Ca, Sr, Ba; B = Mg, group 12, or group 13 metal) when analyzing the structural competition between the $CeCu_2$-type and close-packed Laves phase structures. Interestingly, open packed $CeCu_2$-type phases and close-packed Laves phases occur for the same range of electron counts, 6 to 8 electrons per formula unit (Table 1) [4].

The orthorhombic $CeCu_2$-type (space group *Imma*) [5] features a four-connected three-dimensional framework (Fig. 1) [6]. Each *B*-type atom is surrounded by four neighboring ones in a distorted tetrahedral fashion while *A*-type atoms are sandwiched between two corrugated hexagons from adjacent layers (Fig. 1b). Obviously this structure is electron precise for 8 electrons per formula unit. Examples for polar intermetallics systems with the $CeCu_2$-type are electron precise $SrAl_2$ and $BaIn_2$, and electron deficient $CaZn_2$ and $SrCd_2$. In contrast, Laves phases AB_2 represent close-packed arrangements of differently sized spheres (topological close-packings) and occur in three primary structure types which are closely related (Fig. 2): cubic $MgCu_2$ (space group $Fd\bar{3}m$) and hexagonal $MgZn_2$ and $MgNi_2$ (space group $P6_3/mmc$) [7–9]. Compared to the $CeCu_2$ structure the connectivity of the *B* atom framework in Laves phases is increased to six. The nearest neighbor environment of *A* by 12 *B* atoms corresponds to a truncated tetrahedron (Fig. 2b). Although the Laves phase structures cannot be rationalized by simple electron counting rules there is a clear relationship between electron count and the kind of Laves phase structure adopted. Six-electron systems display the hexagonal $MgZn_2$-type ($CaMg_2$, $CaCd_2$) while 8-electron systems crystallize in the cubic $MgCu_2$-type ($CaAl_2$). Pseudobinary systems ($CaAl_2$–$CaLi_2$, $CaAl_2$–$CaMg_2$, $CaAl_2$–$CaZn_2$) reveal additionally the $MgNi_2$-type for electron counts around 7 [10–13].

* Corresponding author. Fax: +1 480 965 2747.
E-mail address: Ulrich.Haussermann@asu.edu (U. Häussermann).

0022-4596/$ - see front matter © 2008 Elsevier Inc. All rights reserved.
doi:10.1016/j.jssc.2008.07.036

Table 1
Overview of *sp* bonded binary systems with the $CeCu_2$ and Laves phase structures (according to Ref. [4])

	$CeCu_2$-type representatives	Laves phases
6 electron systems	$CaZn_2$, $SrZn_2$, $BaZn_2$, $SrCd_2$, $BaCd_2$, $SrHg_2$, $BaHg_2$	$CaMg_2$, $SrMg_2$, $BaMg_2$, $CaCd_2$ (all $MgZn_2$-type)
8 electron systems	$SrAl_2$, $BaIn_2$	$CaAl_2$ ($MgCu_2$-type)

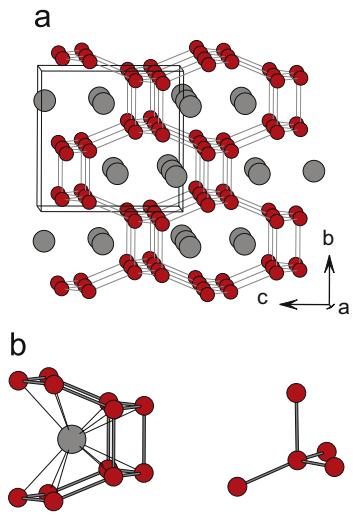

Fig. 1. The orthorhombic $CeCu_2$ structure. Small circles denote *B* atoms, large circles denote *A* atoms. In (b) the nearest neighbor coordination environment for *A* and *B* atoms is shown.

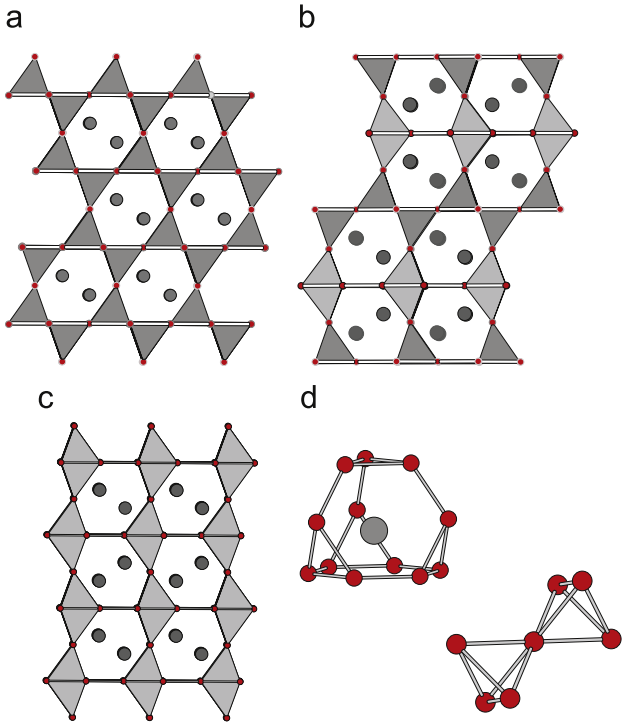

Fig. 2. The Laves phase structure types $MgCu_2$ (defined with respect to a hexagonal unit cell) (a), $MgZn_2$ (b), and $MgNi_2$ (c) projected along the [110] direction. Small circles denote *B* atoms, large circles denote *A* atoms. The *B* atom frameworks are composed of B_4 tetrahedra and B_5 trigonal bipyramids. In (d) the nearest neighbor coordination environment for *A* atoms and *B* atoms involved in B_4 tetrahedra or corresponding to apex atoms in B_5 entities are shown.

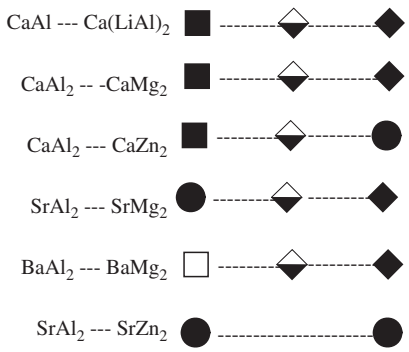

Fig. 3. Phase relations in ternary systems. Filled squares—$MgCu_2$, empty square —$Ba_{21}Al_{40}$, half-filled diamonds—$MgNi_2$, filled diamonds—$MgZn_2$, solid circles—$CeCu_2$.

The factors that govern structural stability between Laves phases and $CeCu_2$-type phases depend critically on the chemical parameters *electronegativity difference* (relating to the polarity of the compound) and *size ratio* between active metal (*A*) and electronegative component (*B*) [14]. The following pairs of compounds exemplify this: $CaAl_2$ (Laves phase)–$SrAl_2$ ($CeCu_2$ phase) and $CaAl_2$ (Laves phase)–$CaZn_2$ ($CeCu_2$ phase). In Fig. 3 relevant 6 to 8 electron systems at the borderline between Laves phases and $CeCu_2$-type phases are compiled. Note that a compound $BaAl_2$ does not exist in the ambient pressure Ba–Al phase diagram but $Ba_{21}Al_{40}$ [12,15].

In previous work, we have established electron concentration-driven Laves phase structural changes in *sp* bonded systems [11,12] and also addressed the question of structural stability with respect to the competing $CeCu_2$ structure [13]. Naturally it is expected that systems with a higher polarity preferably adopt the $CeCu_2$ structure. Indeed, we found that the Allred–Rochow [16] electronegativity difference between *A* and *B* component as single parameter separates sharply Laves phases from $CeCu_2$-type phases at $\Delta EN = 0.45$. Additionally, the low symmetry $CeCu_2$ structure will provide more flexibility with respect to the size ratio r_A/r_B compared to high-symmetry Laves phases, and tolerate combinations between large *A* and small *B* components (as in $SrZn_2$ and $BaZn_2$).

The question arises if the boundary between $CeCu_2$-type phases and Laves phases can be influenced by external parameters. It is well known that polarity or ionicity of compounds diminishes with increasing pressure, and even metal halides become metallic at high pressures [17]. Therefore, the application of high pressure may generally transform open packed $CeCu_2$ phases into close-packed Laves phases. In this respect it would be interesting to see if the relationship between electron count and particular Laves phase structure observed at ambient pressure (cf. Fig. 3) is also followed in potential high-pressure phases. Cordier et al. reported earlier on the synthesis of high-pressure phases of $SrAl_2$ and $BaAl_2$ having the cubic Laves phase structure [18,19]. We reinvestigated these systems by applying different temperature and pressure conditions and extended the study to include $CaZn_2$, $SrZn_2$, and SrZnAl. The latter phases are 6 and 7 electron systems and expected to transform to hexagonal Laves phases with the $MgZn_2$ and $MgNi_2$ structure, respectively.

2. Experimental details

2.1. Synthesis of precursors

The binary compounds $SrAl_2$, $CaZn_2$, and $SrZn_2$ (all $CeCu_2$-type) and $Ba_{21}Al_{40}$ (previously assigned as Ba_7Al_{13} [20]) were prepared from the elements and handled in an Ar-filled glovebox

(O_2 concentration <2 ppm). For $CaZn_2$ and $SrZn_2$, alkaline earth metal (ABCR Karlsruhe, dentritic pieces, 99.9%) and Zn (Alfa Aesar, shots, 99.9999%) were weighed in Ta ampoules (average sample mass about 0.5 g) which were sealed in fused silica Schlenk tubes under reduced pressure. Reactant mixtures were heated to 900 °C for 2 h to ensure complete melting and subsequently quenched in water. After that samples were directly reheated and annealed at 600 °C ($CaZn_2$) and 500 °C ($SrZn_2$) for 7 days, followed again by quenching in water. The silvery grey products could be easily separated as ingots from the Ta tube. For preparing $SrAl_2$ and $Ba_{21}Al_{40}$, elemental mixtures with a slight excess of Al (2 at%) were pressed into pellets, which subsequently were arc melted.

2.2. Multi-anvil synthesis of high-pressure phases

For multi-anvil experiments powdered samples of binary $CaZn_2$, $SrAl_2$, $Ba_{21}Al_{40}$, and $SrZn_2$ and a 1:1 mixture of $SrAl_2$ and $SrZn_2$ (simulating a composition "SrZnAl") were pressed into pellets, which were placed in boron nitride (BN) capsules. Subsequently, the BN capsule (4.55 mm diameter, 2.55 mm long) was positioned with a graphite furnace and a zirconia insulating sleeve in a magnesia octahedron with 14 mm edge length. See Ref. [21] for details. Samples were pressurized to 7–10 GPa in a 6–8 Walker-type multi-anvil high-pressure device with tungsten carbide cubes truncated to 8 mm edge length. After reaching the target pressure the samples were heated to temperatures between 400 and 1000 °C and typically quenched after 1 h by turning off power to the furnace. The preparation of the high-pressure assemblies was performed in air, because the precursor materials are fairly air stable. The recovery of the products, however, was performed in an Ar-filled glove box.

2.3. Structure characterization

To characterize phases and to determine the unit cell dimensions of the high-pressure phases, powder XRD data were collected with a Siemens D-5000 diffractometer (Bragg-Brentano geometry, Cu$K\alpha_1$ radiation, Si added as internal standard). Air sensitive samples were protected by Kapton tape during the XRD measurements. To ensure proper assignment of the indices the observed lines were compared with the calculated ones (program PowderCell [22]) using positional parameters obtained from computational relaxation. Lattice parameters were obtained by least-squares refinement of indexed lines using the program PIRUM [23]. The high-pressure sample of $CaZn_2$ yielded crystals of suitable size for single-crystal X-ray diffraction investigation. Single-crystal intensity data was collected at room temperature on a Bruker SMART APEX system using graphite monochromated Mo$K\alpha$ radiation ($\lambda = 0.71073$ Å) and corrected for Lorentz and polarization effects. SHELXL-97 was used for structure refinement (full-matrix least-squares on F^2) [24]. The structure was refined using the atomic position parameters of the $MgZn_2$ structure (space group $P6_3/mmc$) as starting model. Some details of the single-crystal data collection and refinement are listed in Table 2. Structural parameters are given in Table 3. Further details of the crystal structure investigation may be obtained as supporting information and from Fachinformationszentrum Karlsruhe, D-76344 Eggenstein-Leopoldshafen, Germany (fax: (+49)7247-808-666; e-mail: crysdata@fiz-karlsruhe.de) on quoting the depository number CSD-448878). The high-pressure sample of $SrZn_2$ was subjected to a transmission electron microscope (TEM) study in order to obtain crystallographic information from electron diffraction. A sample was crushed between glass slides, suspended in hexane and then deposited on 3 mm copper grids coated with a holey amorphous carbon film. The so-prepared specimens were then studied in an analytical Philips CM200 FEG (field emission gun) scanning TEM at the John M. Cowley Center for High Resolution Electron Microscopy, Arizona State University, USA operating at 200 kV.

Table 2
X-ray single crystal refinement data for high-pressure $CaZn_2$

Chem formula	$CaZn_2$
Lattice parameters (Å)	
a	5.6393(9)
c	8.994(3)
V (Å^3)	247.43(9)
Space group, Z	$P6_3/mmc$, 4
Formula weight	170.898
λ (Å)	0.71073
D_{calc} (g cm^{-3})	4.586
μ (mm^{-1})	21.032
$R1$, w$R2$	0.051, 0.081

Table 3
Structural parameters for the high-pressure Laves phases of $CaZn_2$ (single-crystal X-ray diffraction), $SrAl_2$ (powder X-ray diffraction), $BaAl_2$ (powder X-ray diffraction) and $SrZn_2$ (first principles computational relaxation)

Chem formula Structure type	$CaZn_2$ $MgZn_2$ (C14)	$SrAl_2$ $MgCu_2$ (C15)	$BaAl_2$ $MgCu_2$ (C15)	$SrZn_2$ $MgZn_2$ (C14)
Lattice parameters (Å)				
a	5.6363(9)	8.2941(4)[a] 8.325(5)[b]	8.672(1)[a] 8.702(5)[c]	5.8945
c	8.994(3)			9.0784
V (Å^3)	247.43(9)	570.56(2)	646.77(5)	273.2
space group, Z	$P6_3/mmc$, 4	$Fd\bar{3}m$, 8	$Fd\bar{3}m$, 8	$P6/_3mmc$, 4
Atomic position parameters				
Type-Wyckoff	Ca 4*f*	Sr 8*a*	Ba 8*a*	Sr 4*f*
x y z	1/3 2/3 0.0592(3)	0 0 0	0 0 0	1/3 2/3 0.0534
Type-Wyckoff	Zn1 2*a*	Al 16*d*	Al 16*d*	Zn1 2*a*
x y z	0 0 0	5/8 5/8 5/8	5/8 5/8 5/8	0 0 0
Type-Wyckoff	Zn2 6 h			Zn2 6 h
x y z	0.8336(2) 2*x* 1/4			0.8423 2*x* 1/4

[a] This work.
[b] Ref [18].
[c] Ref [19].

2.4. Electronic structure calculations

Total energy calculations for $CaAl_2$, $SrAl_2$, $CaZn_2$, and $SrZn_2$ were performed in the framework of the frozen core all-electron projected augmented wave (PAW) [25] method (as implemented in the program VASP [26]). For each composition we considered the structures $MgCu_2$, $MgZn_2$, and $CeCu_2$. The energy cutoff was set to 400 eV. Exchange and correlation effects in all systems were treated by the generalized gradient approximation (GGA), usually referred to as PW91 [27]. The integration over the Brillouin zone was done on special *k*-points determined according to the Monkhorst–Pack scheme [28]. All necessary convergence tests were performed, and total energies were converged to at least 1 meV per atom. For all systems atomic positions and lattice parameters of the considered structures were relaxed for a set of constant volumes until forces had converged to less than 0.01 eV Å^{-1}.

2.5. Diamond anvil cell high-pressure investigations

Single-crystal high-pressure investigations were performed with $CeCu_2$-type $CaZn_2$ using a Merril–Basset type of diamond anvil cell (DAC) with diamond culet diameters of 0.6 mm and

preindented stainless steel gaskets with mechanically drilled hole diameter of about 0.25 mm. A mixture of methanol:ethanol:water (16:3:1) served as pressure transmitting medium. The diffraction measurements were performed with a four-circle diffractometer (Siemens P4/RA) using Mo$K\alpha$ radiation (rotating anode, 5 kW, filament size 0.3 mm × 0.3 mm). Cell parameters were determined from 15 to 20 well-centered reflections in a range of $14^\circ < 2\text{theta} < 30^\circ$. For pressure determination the ruby fluorescence technique [29] and the calibration scale by Mao et al. [30] was applied. The estimated standard deviation for the measured pressure amounts to 0.06 GPa, except for pressures above 8 GPa when it becomes 0.1 GPa (due to fluorescence line broadening)

2.6. Thermal analysis

High-pressure samples of $CaZn_2$, $SrAl_2$, $Ba_{21}Al_{40}$, $SrZn_2$ ($\approx$10 mg) were hermetically sealed in aluminum pans in an Argon atmosphere, and their thermal properties were measured by using a TA 2910 Differential Scanning Calorimetry (DSC) instrument. Indium and tin were employed for the temperature calibration of the instrument. During measurements a helium gas flow of 30 ml min^{-1} was used to prevent oxidation of the sample cans. The scanning range was 40–550 °C at a rate of 10 °C min^{-1}. Measurements were carried out by first holding the samples at 40 °C for 1 min and then heating to 550 °C at 10 °C min^{-1}, equilibrating there for 3 min and then finally cooling to 40 °C at 10 °C min^{-1}. The integrity of the samples after the heating/cooling cycle was ensured by powder X-ray diffraction.

3. Calculational results

We performed first principles calculations to investigate structural competition between the $CeCu_2$-type and Laves phase structures for the systems $CaAl_2$, $SrAl_2$, $CaZn_2$, and $SrZn_2$. As Laves phase structures we considered cubic $MgCu_2$ and hexagonal $MgNi_2$. Fig. 4 summarizes the results in the form of total energy vs volume curves. Note that all four graphs show equally large ranges of ΔE (0.5 eV) and ΔV (20 Å^3) for better comparison.

For the 8 valence electron systems $CaAl_2$ and $SrAl_2$ the cubic $MgCu_2$ structure is preferred over the hexagonal $MgZn_2$ structure, while for the 6 electron systems $CaZn_2$ and $SrZn_2$ the situation is reversed. This is in agreement with the established relationship between electron count and stable Laves phase structure. Hexagonal and cubic Laves phases attain the same equilibrium volume for a particular system. The more open packed $CeCu_2$ structure yields a higher equilibrium volume (by about 5%) compared to the close-packed arrangements. For the $CaAl_2$ system the Laves phase is lowest in energy whereas for the remaining ones it is the $CeCu_2$-type phase. Also this is in accord with the experiment. The stabilization of the $CeCu_2$ structure over a close-packed arrangement increases from $SrAl_2$ to $CaZn_2$ to $SrZn_2$.

Upon compression the total energy for the $CeCu_2$ structure increases faster, and for $SrAl_2$, $CaZn_2$, and $SrZn_2$ its E/V curve crosses that of the close-packed Laves phase structures. From this behavior theory predicts a high-pressure structural transition. At 0 K (which the calculations refer to) $G = E+pV$. The difference in Gibbs-free energy G of two phases 1 and 2 at a given pressure p is given by the difference between intersections of parallel tangents $p = -(\partial E_1/\partial V)_{V=V1} = -(\partial E_2/\partial V)_{V=V2}$ with the ordinate axis. A transformation occurs at a pressure p_{tr} at which the tangents coincide ($\Delta G = 0$). With this so-called common tangent method transition pressures for a $CeCu_2$-type→Laves phase structural change are estimated as 1.8, 4.1, and 8.0 GPa for $SrAl_2$, $CaZn_2$, and $SrZn_2$, respectively.

In summary, theory reproduces correctly the experimental ground state structures for $CaAl_2$, $SrAl_2$, $CaZn_2$, and $SrZn_2$ and predicts pressure-induced structural phase transitions from the $CeCu_2$-type to a Laves phase close packing for the latter systems.

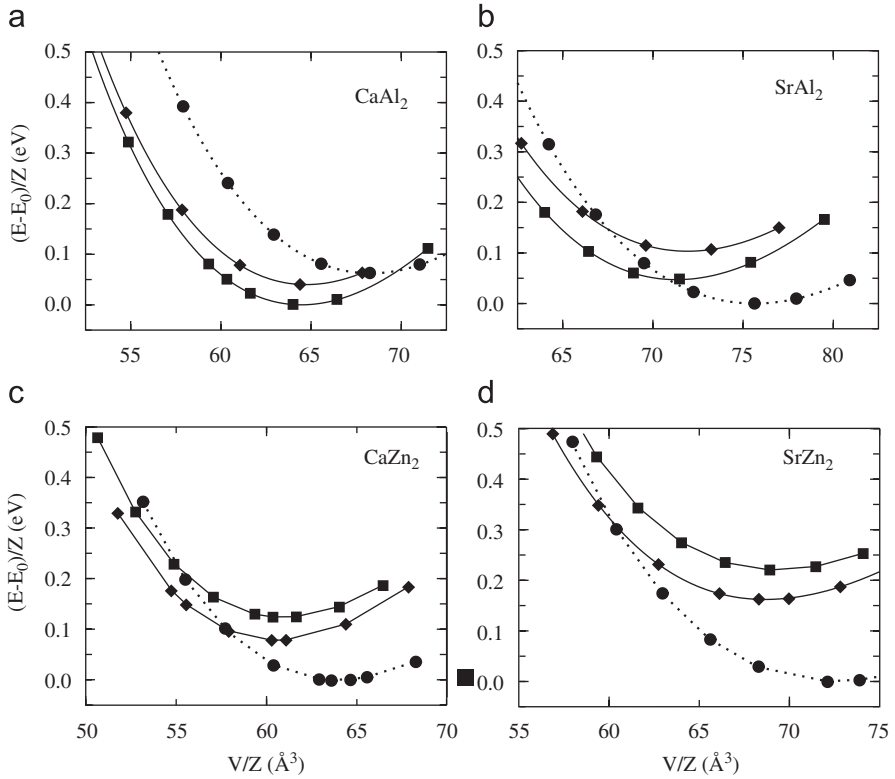

Fig. 4. Total energy vs volume for the systems $CaAl_2$ (a), $SrAl_2$ (b), $CaZn_2$ (c), and $SrZn_2$ (d) in the structure types $MgCu_2$ (squares), $MgZn_2$ (diamonds), and $CeCu_2$ (circles and broken line).

4. Experimental results

4.1. $CaZn_2$

The high-pressure behavior of $CaZn_2$ was first investigated by a single-crystal DAC experiment in a pressure range between 0.5 and 8.5 GPa. This experiment did not indicate a structural transition although pressures well above the theoretically determined transition pressure (4.1 GPa) were applied. The changes of volume and unit cell parameters as a function of pressure are compiled in Fig. 5. The unit cell parameters decrease rather isotropically. Interestingly the *b*-axis, which is the stacking direction of corrugated hexagon layers in the $CeCu_2$ structure is not the most compressible one, but the *c*-axis. The relative volume change was fitted to the Birch Murnaghan equation of states in order to determine the bulk modulus B_0 and its pressure derivative [31]. As a result we obtained $B_0 = 43(2)$ GPa ($B' = 3.8(5)$, $V_0 = 260.5(2)$ Å^3). The bulk modulus of $CaZn_2$ is remarkably low and comparable to elemental Pb.

At first sight it appears surprising that a theoretically predicted phase transition is not observed in a room-temperature DAC experiment. However, there are numerous examples of reconstructive, kinetically hindered, high-pressure phase transitions [32]. When pressurized samples are additionally heated the phase transition usually will take place. Importantly, only kinetically hindered high-pressure phase transitions provide the possibility to quench (metastable) high-pressure phases to ambient pressure.

As a next step we performed multi-anvil high-temperature experiments with $CaZn_2$ and heated a sample that was pressurized at 7 GPa to 1000 °C for 1 h. At these conditions, however, $CaZn_2$ decomposed and the quenched sample corresponded to a complex phase mixture which was not further analyzed. The experiment was then repeated at 700 °C which is about the melting point of $CeCu_2$-type $CaZn_2$ at ambient pressure. At this time $CaZn_2$ transformed quantitatively to a $MgZn_2$-type high-pressure phase, which was recovered at ambient pressure (Fig. 6a). The sample afforded crystals suitable for single-crystal X-ray diffraction studies.

4.2. $SrAl_2$

For $SrAl_2$ the open packed $CeCu_2$ and close Laves phase structure ($MgCu_2$-type) are very close in energy and the theoretically estimated transition pressure is just 1.8 GPa. However, as for $CaZn_2$ a transition is not observable in a room-temperature DAC experiment up to 6 GPa (not shown). Cordier et al. [18] reported earlier on a high-pressure phase of $SrAl_2$ with the cubic Laves phase structure. This phase was obtained by subjecting $SrAl_2$ to a pressure of 6 GPa and a temperature of 1050 °C for 20 min, followed by subsequent quenching. We repeated this experiment using 7 GPa, 1000 °C and a reaction time of 1 h. The quenched sample was highly crystalline and corresponded quantitatively to the $MgCu_2$-type high-pressure phase (Fig. 6b).

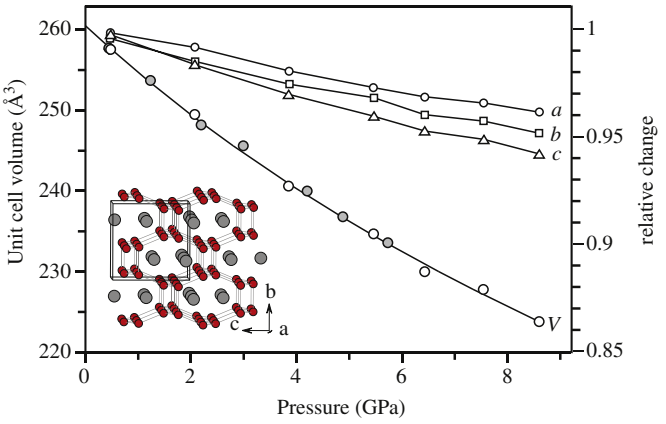

Fig. 5. Volume and lattice parameters of $CeCu_2$-type $CaZn_2$ as a function of pressure according to room-temperature DAC experiments. Absolute values are only given for the volume. The *V*–*P* relation was fit to the third-order Birch-Murnaghan equation and is based on two different experiments (grey and white circles).

4.3. $Ba_{21}Al_{40}$

The ambient pressure binary phase diagram Ba–Al does not contain a phase with a composition "$BaAl_2$" but $Ba_{21}Al_{40}$. Previously Cordier et al. [19] subjected $Ba_{21}Al_{40}$ to 3 GPa and 1000 °C for 5 min. The quenched sample represented a phase mixture from which these authors were able to isolate single crystals of $BaAl_2$ with the $MgCu_2$ structure. Again, we repeated this experiment starting with a pressure of 7 GPa and a temperature of 1000 °C where the sample was kept for 1 h. At these conditions the $Ba_{21}Al_{40}$ starting material decomposed into $BaAl_4$ and presumably a Ba-rich melt. Powder X-ray diffraction did not reveal diffraction lines from another product. Most likely Ba-rich product(s) of the decomposition reaction are X-ray amorphous or formed X-ray amorphous oxides during the decompression and recovery of the high-pressure sample. In similar experiments with $SrZn_2$ (next paragraph) TEM investigations showed small crystallites of SrO in samples that decomposed to $SrZn_5$ or $SrZn_{11}$.

Lowering the temperature to 550 °C yielded quantitatively $BaAl_2$ with the $MgCu_2$ Laves phase structure. The slight Ba excess of the starting materials with respect to the composition AB_2 did not express in a detectable side product. However, compared to $MgCu_2$-type $SrAl_2$ diffraction lines are considerably broader, indicating a less well-crystallized material $BaAl_2$ (Fig. 6c).

4.4. $SrZn_2$

For $SrZn_2$ the energy difference between $CeCu_2$-type ground state and potential high-pressure Laves phase (with the $MgZn_2$ structure in this case) is highest among the investigated systems. When subjecting $SrZn_2$ to 7 GPa and 1000 °C for 1 h the sample decomposed into $SrZn_{11}$ with the tetragonal $BaCd_{11}$ structure and a Sr-rich melt [33]. Interestingly $SrZn_{11}$ is not present in the ambient pressure phase diagram and the formation of this new Sr–Zn phase may be exclusive to high-pressure conditions. When lowering temperature to 550 °C but keeping otherwise conditions constant the crystalline part of the product corresponded to a mixture of hexagonal $SrZn_5$ (space group *P*6/*mmm*) and orthorhombic $SrZn_5$ (space group *Pnma*) [4]. According to TEM studies such decomposed samples contained substantial amounts of SrO. When only applying a reaction temperature of 250 °C at 7 GPa the starting $SrZn_2$ material remained unchanged.

As a next step we increased pressure to 10 GPa (note that the calculated 0 K transition pressure is 8 GPa) and kept $SrZn_2$ at 400 °C for 1 h. Now the initial orthorhombic phase underwent a phase transition to the hexagonal $MgZn_2$-type Laves phase. The X-ray powder pattern matched reasonably well a calculated pattern based on structural parameters obtained form the computational study (Fig. 6d). However, the crystallinity of the high-pressure sample was very poor and lattice parameters could not be refined from the X-ray powder pattern. The phase assignment of high-pressure $SrZn_2$ was therefore attempted with electron microscopy studies. In the TEM high-pressure $SrZn_2$

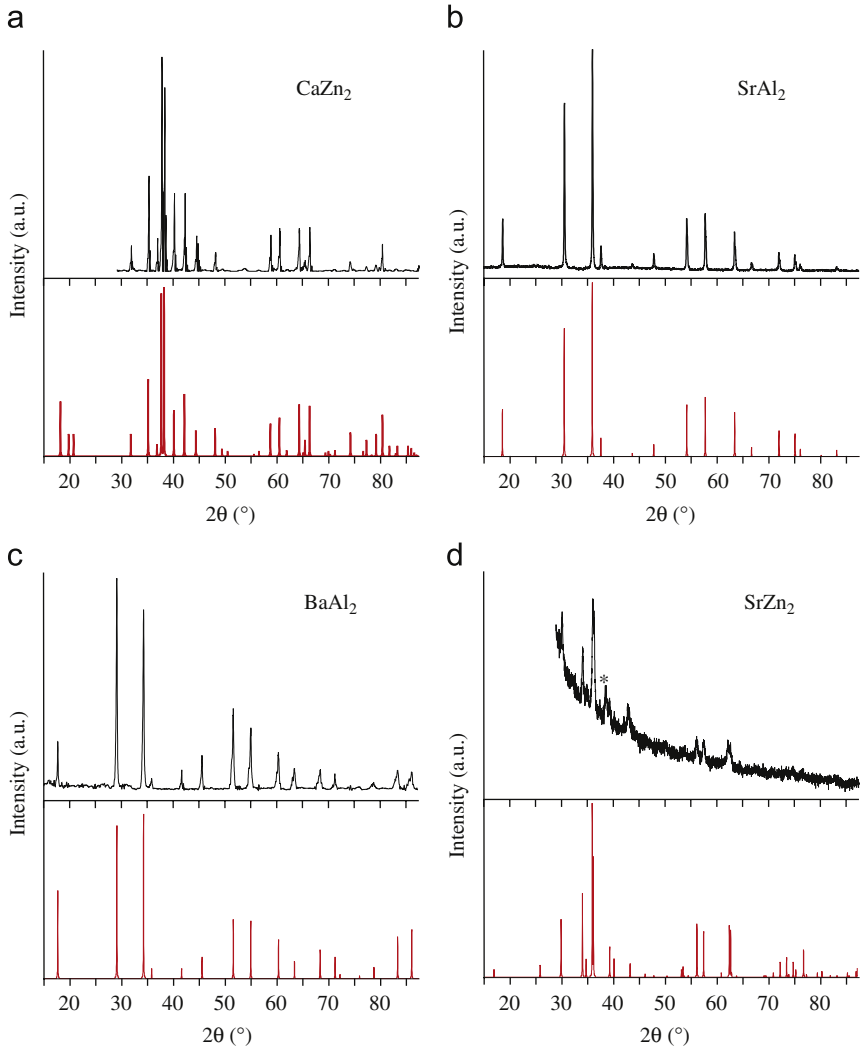

Fig. 6. Diffraction patterns of high-pressure Laves phases for $CaZn_2$ (a), $SrAl_2$ (b), $BaAl_2$ (c), and $SrZn_2$ (d) obtained from multi-anvil experiments. Calculated patterns based on the structural data given in Table 3 are shown in red at the bottom. (Note, for $SrZn_2$ they refer to a computationally relaxed $MgZn_2$ structure.) For $CaZn_2$ and $SrZn_2$ the part of the pattern below $2\theta = 28^\circ$ with large intensity contribution from the protecting Kapton tape has been removed. For $SrZn_2$ no background correction has been attempted. Asterisk mark an impurity peak.

appears as aggregates of small crystals with a maximum size of about 150 nm (Fig. 7a). Fig. 7b shows an electron diffraction pattern taken along the [001] zone axis. Indexing of electron diffraction patterns yields the following *d*-spacings consistent with the hexagonal $MgZn_2$ structure: 5.08 Å (100), 5.09 Å ($1\bar{1}0$), 5.09 Å ($0\bar{1}0$), and 2.93 Å ($\bar{1}10$). The corresponding *a* lattice parameter, 5.86 Å, matches the computationally determined value of 5.89 Å for $MgZn_2$-type $SrZn_2$ and rules out that the pattern was taken from hexagonal $SrZn_5$ which has an *a* parameter of 5.55 Å. Additionally, DSC measurements—as discussed in the next section—showed unambiguously that the obtained product from this reaction corresponded to a metastable high-pressure phase. Attempts to improve the crystallinity of $MgZn_2$-type $SrZn_2$ by increasing the heating time in the multi-anvil experiment proved unsuccessful.

4.5. SrZnAl

1:1 mixtures of $SrZn_2$ and $SrAl_2$ were subjected to 7 GPa and temperatures of 550 and 1000 °C. The aim was to obtain a 7 electron Laves phase system with the $MgNi_2$ structure, similar to ambient pressure phases CaAlZn or CaAlMg. However, products always corresponded to a mixture of $MgCu_2$-type $SrAl_2$ and various Sr–Zn phases. Apparently a ternary compound SrZnAl does not form under high-pressure conditions.

5. Discussion

The polar intermetallics $SrAl_2$, $CaZn_2$, and $SrZn_2$ with the $CeCu_2$ structure, as well as $Ba_{21}Al_{40}$ transform to AB_2 Laves phases in multi-anvil experiments. These high-pressure phases can be recovered at ambient conditions and their structural parameters are compiled in Table 3. Recoverable high-pressure phases imply that the involved phase transition is kinetically hindered; pressure and temperature have to be applied simultaneously for the formation of the high-pressure phase. With temperature, however, different phase relations may apply and the AB_2 composition may not be stable above a certain temperature. Only $SrAl_2$ forms the high-pressure phase at temperatures (1000 °C) above the peritectic melting temperature of the ambient pressure phase (936 °C). For $SrZn_2$ reaction temperatures should be even lower

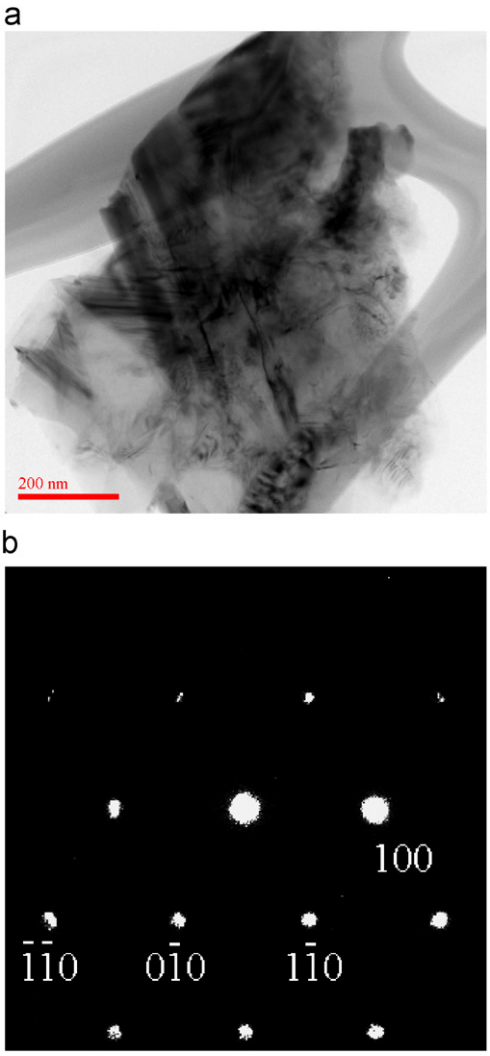

Fig. 7. Bright field TEM image (a) and electron diffraction pattern (b) of high-pressure $SrZn_2$.

(below 450 °C) than the melting point of $CeCu_2$-type phase (575 °C) in order to maintain the composition AB_2. The crystallinity of the Laves phase products decrease with decreasing reaction temperature.

The high-pressure phases for $SrAl_2$ and $BaAl_2$ have been previously reported [18,19]. Our work confirms the result of these earlier studies. Additionally we could show that in the case of $BaAl_2$ the application of a lower reaction temperature leads to a single-phase product. Our lattice parameters are by 0.03 Å smaller that those reported by Cordier et al. (cf. Table 3). The series of Laves phases $CaAl_2$, $SrAl_2$, and $BaAl_2$ is interesting. The Al–Al distance in the *B* atom framework of the $MgCu_2$ structure increases from 2.84 to 2.93 to 3.07 Å. The latter distance appears as extremely strained taking the Al–Al nearest neighbor distance in *fcc* Al as a reference (2.86 Å). Al–Al distances in ambient pressure $CeCu_2$-type $SrAl_2$ [34] and $Ba_{21}Al_{40}$ [12]—where Al frameworks with lower connectivity are realized—range from 2.78 to 2.93 Å and 2.64 to 2.99 Å, respectively.

High-pressure Laves phases of polar intermetallics follow the electron count-driven structural variations established for ambient pressure systems [10–13]. Eight electron systems adopt the $MgCu_2$ structure whereas 6 electron systems crystallize in the $MgZn_2$ structure. Thus, with pressure the system $CaAl_2$–$CaZn_2$ [13] behaves analogous to $CaAl_2$–$CaMg_2$ [11] displaying the sequence $MgCu_2 \rightarrow MgNi_2 \rightarrow MgZn_2$ with decreasing electron count (cf. Fig. 3). For $SrAl_2$–$SrZn_2$ no intermediate (ternary) Laves phase (with the $MgNi_2$ structure) could be found.

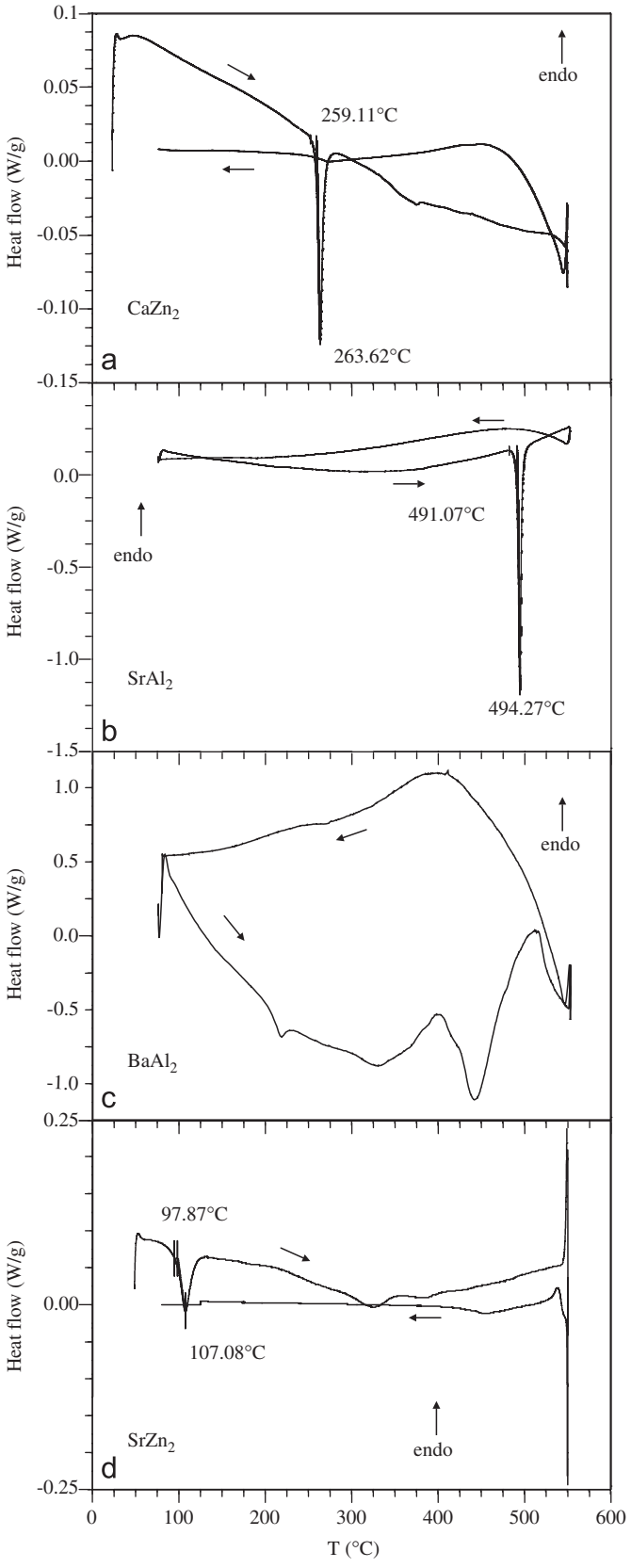

Fig. 8. DSC traces for the high-pressure Laves phases of $CaZn_2$ (a), $SrAl_2$ (b), $BaAl_2$ (c), and $SrZn_2$ (d).

Finally the thermal stability of the high-pressure Laves phases of $CaZn_2$, $SrAl_2$, $BaAl_2$, and $SrZn_2$ were studied up to 550 °C by DSC measurements (Fig. 8). All traces exhibited exothermic events, which confirms the metastable nature of these phases. The samples were subsequently examined by X-ray powder diffraction and the diffraction patterns showed quantitatively restituted $CeCu_2$-type phases for $CaZn_2$, $SrAl_2$, and $SrZn_2$, and $Ba_{21}Al_{40}$ for $BaAl_2$. With the applied measurement conditions the high-pressure phases of $CaZn_2$ and $SrAl_2$ revert to the ground state at about 260 and 490 °C, respectively. The exothermic peaks are very sharp, which is in contrast to $BaAl_2$ and $SrZn_2$. The latter high-pressure phases possess very strained *B* atom networks due to the large size of the *A* component. Additionally for $BaAl_2$ the stoichiometry is different in the ambient pressure phase. The transformation to $Ba_{21}Al_{40}$ may therefore not proceed as a single step and the heating curve displays several events (around 200 and 400 °C). For $SrZn_2$ the transition from the high-pressure phase to the ground state occurs already around 100 °C and expresses as a broad peak in the DSC trace. This may be related to the microcrystalline nature of the sample. Despite the low transition temperature, crystals of $MgZn_2$-type $SrZn_2$ remained stable under the electron beam during electron microcopy investigations (cf. Fig. 7).

In conclusion, we propose that for $CeCu_2$-type polar intermetallics Laves phase structures are competing structures. Both types of structures are realized for the same range of valence electron concentration, i.e. 6–8 electrons per formula unit. The boundary between open packed, polyanionic, $CeCu_2$-type phases and close-packed Laves phases is primarily governed by the electronegativity difference between the *A* and *B* component. The application of pressure has the effect of decreasing the electronegativity difference between components in binary systems. Thus $CeCu_2$-type polar intermetallics can be compressed into Laves phases. High-pressure Laves phases are quenchable and their structures follow the electron count controlled relationships for *sp* bonded systems established previously.

Acknowledgments

This work was supported by the Carl Trygger foundation for Scientific Research (Sweden) and the ACS Petroleum Research Fund (USA) under Grant no. 45796-AC10.

Appendix A. Supplementary data

Supplementary data associated with this article can be found in the online version at doi:10.1016/j.jssc.2008.07.036.

References

[1] (a) J.D. Corbett, Angew. Chem. Int. Ed. 39 (2000) 670;
(b) J.D. Corbett, Inorg. Chem. 39 (2000) 5178;
(c) J.D. Corbett, in: S.M. Kauzlarich (Ed.), Chemistry, Structure and Bonding of Zintl Phases and Ions, VCH, New York, 1996, pp. 139–181.
[2] G. Cordier, B. Eisenmann, in: S.M. Kauzlarich (Ed.), Chemistry, Structure and Bonding of Zintl Phases and Ions, VCH, New York, 1996, pp. 61–137.
[3] The $BaAl_4$ structure is a prominent example of a "robust" polar intermetallic structure type; see e.g. U. Häussermann, S. Amerioun, L. Eriksson, C.-S. Lee, G.J. Miller, J. Am. Chem. Soc. 124 (2002) 4371.
[4] P. Villars, L.D. Calvert, Pearsons Handbook of Crystallographic Data for Intermetallic Compounds, second ed., ASM International, Materials Park, OH, 1991 (and Desk Edition, 1997).
[5] A.C. Larson, Acta Crystallogr. 14 (1961) 73.
[6] G. Nuspl, K. Polborn, J. Evers, G.A. Landrum, R. Hoffmann, Inorg. Chem. 35 (1996) 6922.
[7] F. Laves, Naturwissenschaften 27 (1939) 65.
[8] F. Stein, M. Palm, G. Sauthoff, Intermetallics 12 (2004) 713.
[9] (a) B.G. Hyde, S. Andersson, Inorganic Crystal Structures, Wiley, New York, 1989;
(b) U. Müller, Inorganic Structural Chemistry, Wiley, Chichester, 1993.
[10] R. Nesper, G.J. Miller, J. Alloys Compd. 197 (1993) 109.
[11] S. Amerioun, S.I. Simak, U. Häussermann, Inorg. Chem. 42 (2003) 1467.
[12] S. Amerioun, T. Yokosawa, U. Häussermann, Inorg. Chem. 43 (2004) 4751.
[13] K. Söderberg, M. Boström, Y. Kubota, T. Nishimatsu, R. Niewa, U. Häussermann, Y. Grin, O. Terasaki, J. Solid State Chem. 179 (2006) 2690.
[14] W. Harms, M. Wendorff, C. Röhr, Z. Naturforsch. 62b (2006) 177.
[15] T.B. Massalski (Ed.), Binary Alloy Phase Diagrams, second ed., ASM International, Materials Park, OH, 1990.
[16] A.L. Allred, E.G. Rochow, J. Inorg. Nucl. Chem. 5 (1958) 264.
[17] S.S. Batsanov, J. Phys. Chem. Solids 58 (1997) 527.
[18] G. Cordier, E. Czech, H. Schäfer, Z. Naturforsch. 37b (1982) 1442.
[19] G. Cordier, E. Czech, H. Schäfer, Z. Naturforsch. 39b (1984) 421.
[20] M.L. Fornasini, G. Bruzzone, J. Less-Common Met. 40 (1975) 335.
[21] K. Leinenweber, J. Parise, J. Solid State Chem. 114 (1995) 277.
[22] W. Kraus, G. Nolze, J. Appl. Cryst. 29 (1996) 301.
[23] P.-E. Werner, Ark. Kemi 31 (1969) 513.
[24] G.M. Sheldrick, SHELXL97, University of Göttingen, Germany, 1997.
[25] (a) P.E. Blöchl, Phys. Rev. B 50 (1994) 17953;
(b) G. Kresse, J. Joubert, Phys. Rev. B 59 (1999) 1758.
[26] (a) G. Kresse, J. Hafner, Phys. Rev. B 47 (1993) RC558;
(b) G. Kresse, J. Furthmüller, Phys. Rev. B 54 (1996) 11169.
[27] J.P. Perdew, Y. Wang, Phys. Rev. B 45 (1992) 13244.
[28] H.J. Monkhorst, J.D. Pack, Phys. Rev. B 13 (1976) 5188.
[29] G.J. Piermarini, S. Block, J.D. Barnett, R.A. Forman, J. Appl. Phys. 46 (1975) 2274.
[30] H.K. Mao, J. Xu, P.M. Bell, J. Geophys. Res. B 91 (1986) 4673.
[31] (a) F.D. Murnaghan, Finite Deformation of an Elastic Solid, Wiley, New York, 1951;
(b) F. Birch, J. Appl. Phys. 9 (1938) 279;
(c) F. Birch, Phys. Rev. 71 (1947) 809;
(d) F. Birch, J. Phys. Chem. Solids 38 (1977) 175;
(e) F. Birch, J. Geophys. Res. 83 (1978) 1257.
[32] (a) L. Vocadlo, G.D. Price, I.G. Wood, Acta Crystallogr. B 55 (1999) 484;
(b) L. Vocadlo, G.D. Price, I.G. Wood, Acta Crystallogr. B 56 (2000) 369;
(c) D.P. Dobson, L. Vocadlo, I.G. Wood, Am. Mineral. 87 (2002) 784;
(d) D.C. Palmer, R.J. Hemley, C.T. Prewitt, Phys. Chem. Miner. 21 (1994) 481;
(e) A. Lazicki, C.-S. Yoo, W.J. Evans, W.E. Pickett, Phys. Rev. B 73 (2006) 184120.
[33] S. Kal, E. Stoyanov, T.L. Groy, U. Häussermann, Acta Crystallogr. C 63 (2007) i96.
[34] G. Nagorsen, H. Posch, H. Schäfer, A. Weiss, Z. Naturforsch. 24b (1969) 191.